Coastal Engineering 163 (2021) 103775

Contents lists available at ScienceDirect

Coastal Engineering

journal homepage: http://www.elsevier.com/locate/coastaleng

Runup on a vertical column in strong water wave events

John Grue *, Bodgan Osyka

Mechanics Division, Department of Mathematics, University of Oslo, Oslo, Norway

ARTICLE INFO

Keywords:
Runup
Vertical column
Non-breaking waves
Breaking waves
Finite depth
Great depth

ABSTRACT

Runup on a slender cylindrical column exposed to long, steep waves, at finite and great depth is quantified by high speed camera technique in wave channel. Ratio between water depth (h) and cylinder diameter (D) is $h/D = 10, 4.16, 2.5$. Breaking and non-breaking wave events are made by focusing technique. The trough-to-trough period (T_{TT}), crest height ($\eta_{0,m}$), frequency ($\omega = 2\pi/T_{TT}$) and reference speed (g/ω) of each wave event are defined (g denotes acceleration of gravity). Wavenumber (k) is obtained from the dispersion relation. Experimental runup maximum (Ru_m) is presented in terms of variable $Z = [2\omega^2(Ru_m - \eta_{0,m})/g]^{1/2}$. Measurements at finite water depth collapse along a linear relationship $k\eta_{0,m} = a + b\,Z$ where coefficients are obtained from the experiments. Results from other studies including large scale measurements fit to this curve, for $h/D < 5$, $kh < 2$ and $kD < 0.52$. Results at great water depth with $h/D = 10$ show, beyond a threshold wave slope, a similar relationship. Growth factor ($1/b$) is then much stronger. Gradual transition between results at finite depth and great water depth occurs for $5 < h/D < 10$ and $kh > 2.5$. Measured runup velocity along the column is up to 1.8 times the reference speed at great depth ($h/D = 10$) and up to 1.2 times the reference speed at finite depth. Wave slope $k\eta_{0,m}$ is up to 0.56.

1. Introduction

Vertical columns are used as support of a variety of offshore geometries including wind turbine foundations at sea, offshore platforms, or other installations. Of current actuality is the growing industry of offshore wind farms where the Dogger Bank project represents a newcomer. The recent contract to Equinor and SSE Renewables concerns the construction of a total installed capacity of 3.6 GW. The columns supporting the wind turbines will stand on a water depth of 20 m–35 m. With a pile diameter of 8 m, water depth to diameter ratio is in the range 2.5–4.37. Offshore columns are exposed to non-breaking or breaking waves. The motion poses loads and causes runup on the geometries. The runup motion may destroy equipment mounted along the vertical legs. The vertical water motion and jets caused by the wave-body interaction may cause local damage of, e.g., platform deck, where the margin of the air gap is an essential parameter. Faltinsen et al. (2004) have noted that the description of wave runup is not state-of-the-art. They suggest that both horizontal and vertical loads are considered. Runup as well as its velocity are important quantities.

De Vos et al. (2007) and Lykke Andersen et al. (2011) have listed several reasons why runup on slender vertical cylinders caused by breaking and non-breaking waves are important. They performed wave tank experiments at small scale. Wave runup on piles due to random waves at finite depth was measured using resistance type wave gauges. Later, Ramirez et al. (2013) performed experiments in the large wave channel in Hannover. Runup on a pile in random waves was measured by several techniques. Video camera technique, eventually used in a repetition of the experiments, was used to define three runup levels, where level A corresponds to the green water run-up (thick layer), level B to runup of thin layer of water and air mixture, and water layer which was no longer attached to the surface of the pile, or high spray concentration, and level C to maximum spray. Present high-speed camera recordings of the runup at small scale is equivalent to level B runup. Scale effects were by Ramirez et al. found to be minor. In Garborg et al. (2019) the large scale runup data of Ramirez et al. (2013) were reanalyzed. Garborg et al. suggested that measured data at small scale using wire type gauges should be considered as inaccurate, and only be sufficient for level A runup. Further, they suggested that video recordings were superior to the wire type gauge technique. Garborg et al. suggested four different procedures of postprocessing of the measurements. While the zero-crossing period of individual wave events was given, the crest height was not. Rather, the crest height and horizontal velocity below crest were calculated using ideal theory of periodic waves on flat bottom (Fenton, 1988). The predictions were used to express the runup in terms

* Corresponding author.
E-mail address: johng@math.uio.no (J. Grue).

https://doi.org/10.1016/j.coastaleng.2020.103775
Received 20 December 2019; Received in revised form 17 June 2020; Accepted 17 August 2020
Available online 26 August 2020

of the modified stagnation head assumption.

Myrhaug and Holmedal (2010) developed a statistical, theoretical approach of the wave runup comparing to data from De Vos et al. (2007). Recently, Kazeminezhad and Etemad-Shahidi (2015) used data mining approach to express runup in terms of the wave steepness, where the latter was defined by the wave height. Bonakda et al. (2016) performed runup measurements in non-breaking periodic waves in the long wave regime ($kh < 0.5$, k wavenumber, h water depth). Results were expressed in terms of the wave height. Fully nonlinear time-domain boundary element model (ANSWAVE) and second-order time-domain boundary element model (WAVETANK) were used to calculate runup on wide bottom-mounted cylinder at intermediate depth, at low wave slope and Froude number (Buchmann et al., 2000). Zhang and Teng (2017) performed calculations for a wide cylinder exposed to cnoidal waves in shallow water. Morris-Thomas and Thiagarajan (2004) used the WAMIT program (wamit,inc.) to calculate the second-order runup for deep water conditions. Their complementary wave tank experiments were performed for finite depth conditions. Works that concern wave impact and air gap include Stansberg et al. (2005), where linear and second-order numerical models and physical wave tank tests were combined.

1.1. Physical processes and key parameters for runup

Offshore wind turbine developments concern waves that are long (wavelength $\lambda = 2\pi/k$) compared to the cylinder diameter (D). This means that kD is small. A water depth h in the range 20–40 m and cylinder diameter of, e.g., $D = 8$m implies a ratio $h/D \sim 2.5$–5. If the energetic waves have a wavelength of 300 m (or 100 m), corresponding parameter kh for $h = 40$m is 0.84 (or 2.56). Nonlinear waves are characterized by the wave slope. This is here estimated by $k\eta_{0,m}$ where $\eta_{0,m}$ denotes the crest height. Strongly nonlinear waves are limited by breaking where $k\eta_{0,m} < 0.56$ in present experiments. Runup events on slender cylinders at finite depth are governed by the following nondimensional parameters and ranges:

$$h/D \sim 2.5 - 5, \quad kh \sim 0.84 - 2.56, \quad kD < 0.5, \quad k\eta_{0,m} < 0.56.$$

Standard wave diffraction and radiation analysis programs such as WAMIT (wamit.inc) may be used for linear and second-order calculations of the runup on slender piles. Method is valid for small and moderate wave slope. Linear periodic waves of amplitude A interacting with a slender cylinder produces a runup maximum of $Ru_m = A(1 + kD/2)$ and is calculated for a slender cylinder using linear long wave approximation from Newman (1977, eq. 6.163). Second-order calculations using WAMIT show that $Ru_m = Af_1 + A^2 f_2$ in periodic waves where f_1 and f_2 are functions of h/D, kh and kD. Such calculations by Morris-Thomas and Thiagarajan (2004, Fig. 9b) compare excellent to experiments for wide cylinders ($h/D = 5$, $kD = 1.4$) and $kA < 0.3$. Calculations and measurements for a slender cylinder ($h/D = 5, kD = 0.43$) fit with second-order theory for $kA < 0.15$. For larger wave slope ($kA > 0.15$) the experimental runup grows at a much faster rate compared to prediction (Morris-Thomas and Thiagarajan, 2004, Fig. 9c). However, the runup is still found to grow with the amplitude squared in their case. On the other hand, experimental coefficient f_2 becomes much greater compared to the second order prediction. The deviation between experiment and second-order theory takes place at a threshold wave slope. The threshold wave slope is function of h/D, kh and kD, as confirmed by present experiments. Similar behaviour is found for the horizontal orbital velocity in breaking or near-breaking waves (Grue and Jensen, 2012) and the Stokes drift in breaking waves (Lenain et al., 2019).

Laboratory experiments (Hallermeier, 1976) have suggested that the orbital velocity of the input wave is an important parameter to the strongly nonlinear flow past a thin pile. Runup is discussed in terms of a relation that may be obtained from a variant of the energy equation (e.g., De Vos et al., 2007; Lykke-Andersen et al., 2011; Garborg et al., 2019):

$$Ru_m - \eta_{0,m} = \frac{1}{2} M u_m^2/g. \quad (1)$$

Here, u_m denotes crest velocity of the incoming wave and M is a proportionality factor. Much work has concerned predictions using this relation.

1.2. Present experiments

In present experiments, time sequences of the runup on vertical cylinder are recorded by high-speed camera technique and digitalized. Maximum runup, time series of the runup and its velocity are obtained. The runup we measure corresponds to level B in Ramirez et al. (2013), Garborg et al. (2019), see section 2.1 for definition and clarification. The cylinder diameter is $D = 6$cm. The water depth is either $h = 15$cm, 25 cm or 60 cm making a depth to diameter ratio of $h/D = 2.5 - 4.16$ in the finite depth cases, and $h/D = 10$ in the deep water case. Waves are shallow or at intermediate depth with $kh \sim 0.65 - 2.17$, or at great water depth with $kh \sim 2 - 4.5$. The wavelength is great compared to the cylinder diameter with $0.18 < kD < 0.52$.

The time series of the input waves are used to define the crest height ($\eta_{0,m}$) and the trough-to-trough period (T_{TT}) of the strong wave events. Frequency (ω), reference speed (g/ω) and wave slope of the event are thereby defined, for subsequent references and discussion of the runup measurements.

Following the Introduction, we describe in section 2 the experimental method and provide definitions of the input waves. Results for the runup with comparisons particularly to the large scale measurements of Ramirez et al. (2013) and Garborg et al. (2019) are given in section 3. Runup velocity is studied in section 4. Conclusions are given in section 5.

2. Experimental method and definitions

The experiments were performed in a 25 m long and 0.5 m wide wave channel in the Hydrodynamics Laboratory at the University of Oslo. A vertical cylinder of diameter $D = 6$cm was positioned 10.86 m from the wave maker and 10.23 m from an absorbing beach of length 3.51 m, at the opposite end of the channel. The water depth h was 0.6 m, 0.25 m or 0.15 m giving depth to cylinder diameter ratios of 10, 4.16 and 2.5, respectively. Focusing waves were generated using standard techniques (e.g. Baldock et al., 1996; Grue et al., 2003). The elevation of the incoming waves was measured by ultra sound UltraLab ULS Advanced system. This combines one transmitting sensor and two receiving sensors operating at 250 Hz. The elevation was measured at the position of the cylinder axis with the cylinder absent.

Runup on the cylinder was filmed using Photron's FASTCAM SA5 High-Speed Video System (www.photron.com) (Fig. 1a). A frame rate of 500 fps was used, where the camera provides up to 7 500 fps. The resolution is 1 024 times 1 000. The VLX2 LED Line Lightning (Gardasoft Vision) light source used in the recordings has maximum intensity of 2.3×10^6 Lux (Fig. 1a). The intensity of the led lamp is in the range from 0% to 140%, where 140% corresponds to maximum intensity. The light intensity was controlled and adjusted using the Tera Term terminal software. We have also obtained the overturning moment on the cylinder (with respect to the bottom) using force transducers HBM (www.hbm.com). Only a few results of the overturning moment are included for illustrative purposes.

The sensors and camera were mapped against each other using analog trigger circuitry (ATC). The ATC generated an internal trigger signal to initiate the acquisition (www.ni.com). This was monitored relative to the paddle motion obtaining at syncronized time the input wave elevation, and in the repeated experiments, the runup motion and overturning moment. The recordings were obtained long before any small reflections from the beach occurred at the position of the cylinder.

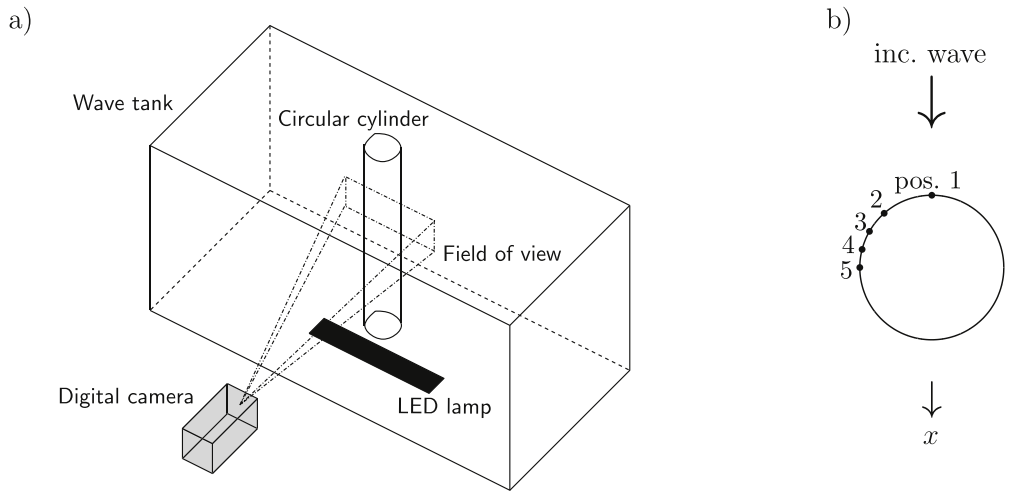

Fig. 1. a) Sketch of wave channel, vertical cylinder, illumination, camera position, field of view. B) Positions 1–5 along the cylinder contour where run-up $Y_i(t)(i = 1,..5)$ is obtained. Incoming waves are directed along the x-axis.

2.1. Runup

Snapshots of the wave runup along the cylinder are shown at two instants. The first is at maximum overturning moment, the second at maximum runup at the weatherside (Fig. 2c and d). A meter indicating distance in cm was printed on thin paper and checked versus a steel ruler. The meter, visible in the figures, was accurately mounted in vertical position on the outward face of the cylinder by transparent tape. The runup was extracted manually from each single image of the video sequence. In each image, the location of the runup along the cylinder surface including droplets was very clear. This corresponds to runup level B as defined in the large scale tests by Ramirez et al. (2013). The collection of vertical positions from the images provides the runup as function of time.

Let x denote the coordinate along the wave direction with $x = 0$ at the cylinder axis (Fig. 1b). The runup was obtained at five positions along the cylinder contour with x-coordinates: $x_1 = -D/2$ (position 1), $x_2 = -(3/4)(D/2)$ (position 2), $x_3 = -(1/2)(D/2)$ (position 3), $x_4 = -(1/4)(D/2)$ (position 4) and $x_5 = 0$ (position 5). In terms of the angle along the cylinder contour, position 1 is at the weather side at an angle of 0°, position 2 at 41.4°, position 3 at 60°, position 4 at 75.7° and position 5 at 90°. We denote the runup above mean water level at positions 1–5 by $Y_i(t)$, $i = 1$–5. These were obtained at time intervals of 0.01 s corresponding to every fifth image. We denote by $Ru_m = \max(Y_1(t))$ on the weather side. The data from the runs are organized according to decaying $Ru_m/\eta_{0,m}$. ($\eta_{0,m}$ denotes the crest height of the

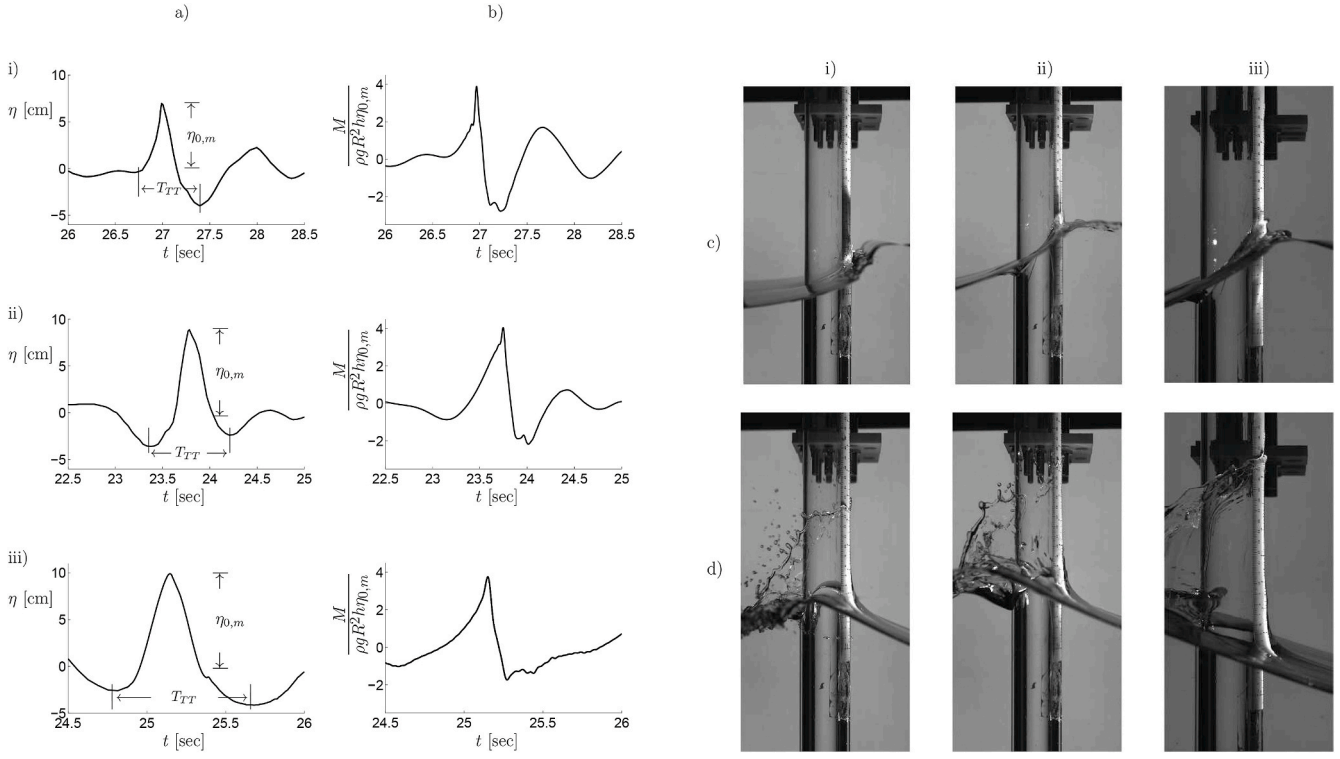

Fig. 2. a) Elevation and b) overturning moment. c) Video recording of elevation at force maximum, and d) at run-up maximum. Deep water cases: D21 (i) and D11 (ii); finite depth case: H131 (iii). In a) crest height $\eta_{0,m}$ and trough-to-trough period T_{TT} indicated.

incoming wave at the position of the cylinder axis.) Note that $\eta_{0,m}$ was determined with the cylinder absent. The experiments were repeated with the cylinder present (Tables 1 and 2).

2.2. Input waves and definitions

A number of twenty six focusing wave events were produced in the wave channel. Ten of them were obtained with a water depth of $h = 60$cm ($h/D = 10$), another ten runs with a water depth of $h = 25$cm ($h/D = 4.16$) and then six runs with $h = 15$cm ($h/D = 2.5$), see Tables 1 and 2 Time series of the wave elevation ($\eta_0(t)$) were recorded at the position of the cylinder axis, with the cylinder absent. Large breaking and non-breaking wave events were produced by focusing technique. Large wave events in focused and random waves are similar (Grue et al., 2003; Grue and Jensen, 2012). Following these two references, we define from the time series of the input wave elevation, the trough-to-trough period (T_{TT}) and the crest height ($\eta_{0,m}$). Index zero indicates measurement without the cylinder present, and index m maximum elevation.

The experiments were then repeated, with the cylinder mounted at the predefined location. The time series of $\eta_0(t)$, overturning moment ($M(t)$) on the cylinder with respect to the bottom, and runup motion filmed by the high-speed camera were all syncronized relative to the paddle motion. Results for T_{TT}, $\eta_{0,m}$ and maximum overturning moment are given in Tables 1 and 2 Time series of $\eta_0(t)$ and $M(t)$ are shown in Fig. 2a and b for the strongest deep water case D21 (plots i), another strong deep water case D11 (plots ii) and the strongest, non-breaking case H131 (plots iii). The crest height $\eta_{0,m}$ is a clearly defined measure. So is the trough-to-trough period T_{TT} where this is clearly defined from the elevation in Fig. 2a, cases ii) and iii). In the strongest case in Fig. 2a plot i) which is a non-breaking wave, where the wave breaks right behind the cylinder position, the period T_{TT} is also well defined. We further note that there is a close correspondence between the trough-to-trough period of the elevation and zero-up crossing period of the time series of the overturning moment.

In each wave event we define a frequency by $\omega = 2\pi/T_{TT}$. In the deep water case we follow Grue et al. (2003), Grue and Jensen (2012), with subsequent tests given by Stansberg et al. (2006) and Alberello et al. (2018). For each wave event we define:

$$k\eta_{0,m} = \varepsilon + \frac{1}{2}\varepsilon^2 + \frac{1}{2}\varepsilon^3, \tag{2}$$

$$\omega^2 = gk\left(1+\varepsilon^2\right), \tag{3}$$

where k defines the wavenumber and ε the wave slope corresponding to kA for Stokes waves (of amplitude A). From (2)-(3) we define a reference wave propagation speed of the deep water wave event by

$$c_{ref}^{\infty} = \omega/k = \sqrt{\left(g/k\right)(1+\varepsilon^2)} = \left(g/\omega\right)(1+\varepsilon^2). \tag{4}$$

The c_{ref}^{∞} is used to scale the horizontal particle velocity at the wave crest (u_m). Measurements of random bidirectional field waves as well as laboratory recordings of unidirectional irregular waves, and calculations, are summarized by Grue and Jensen (2012, Fig. 9) obtaining that

$$u_m \Big/ c_{ref}^{\infty} \simeq \varepsilon e^{k\eta_{0,m}} \Big/ \sqrt{1+\varepsilon^2}, \quad \varepsilon < 0.39. \tag{5}$$

This covers the steepness range of the present experiments at great water depth. The function (5) is shown in Fig. 3b. The ratio between the orbital velocity at crest and linear deep water wave speed, $u_m/(g/\omega)$, is another monotoneous function of the wave slope. We shall use this ratio in the discussion of the runup at great depth.

At finite water depth, the linear, horizontal orbital velocity of progressive waves reads $u = (\partial/\partial x)(Ag/\omega)(\cosh k(y+h)/\cosh kh)\sin(kx-\omega t)$ (x horizontal coordinate, y vertical coordinate), where $\omega^2 = gk\tanh kh$ connects ω and k. At wave crest this gives $u = Ak(g/\omega)$, or $u/(g/\omega) = Ak$. The ratio grows with the wave slope and is independent of the water depth. We shall use the ratio $u/(g/\omega)$ also in the discussion of the runup at finite water depth.

We define g/ω– the deep water linear wave celerity – as reference speed in the analysis of the runup on the cylinder, both in the deep water case and in the finite depth case. The wave slope of each wave event is characterized by $k\eta_{0,m}$. In deep water $k\eta_{0,m}$ is obtained by (2–3). At finite water depth the wavenumber is obtained from the linear dispersion relation. This is then multiplied by $\eta_{0,m}$.

3. Results for runup

A slight modification of (1) is introduced where first factor $2g$ is multiplied on each side of the equation and then the square root is taken. The result is divided by reference speed (g/ω) obtaining

$$Z = \left[2\omega^2\left(Ru_m - \eta_{0,m}\right)\Big/g\right]^{1/2} = M^{1/2}u_m\Big/(g/\omega). \tag{6}$$

The relation defines the variable Z. This is studied in terms of the wave slope $k\eta_{0,m}$. Function Z depends further on variables h/D, kh and kD.

3.1. Great water depth ($h/D = 10$)

Experiments with depth to cylinder ratio of $h/D = 10$ ($h = 60$ cm) are first considered. The cylinder is slender with $kD \sim 0.2$– 0.45. The runup $Ru_{0,m}/\eta_{0,m}$ and runup function Z in (6) exhibit one behaviour up to $k\eta_{0,m} = 0.355$. Another behaviour is observed for the range $0.355 < k\eta_{0,m}$ where both $Ru_m/\eta_{0,m}$ and Z grow linearly with the wave slope. (Fig. 3a and b). The physics of the two ranges obviously differ. We have included in the plot, second-order calculations of the runup on a cylinder exposed to periodic waves in water of infinite depth and $kD = 0.416$. The calculations were made by Morris-Thomas and Thiagarajan (2004) using WAMIT. The draught of the cylinder was $2.9D$ (and $h = \infty$ in the calculations). The results illustrate that second-order wave diffraction theory models the wave-cylinder interaction process up to a threshold

Table 1
Runs at water depth $h = 60$cm ($h/D = 10$). [1]Breaking; [1]weakly breaking; [3]non-breaking.

run	T_{TT}[sec.]	$\eta_{0,m}$[cm]	$k\eta_{0,m}$	ε	$Ru_m/\eta_{0,m}$	kD	$M_m/\rho gR^2\eta_{0,m}h$	kh
D22[1]	0.69	6.62	0.487	0.385	2.42	0.442	3.69	4.42
D21[1]	0.70	6.93	0.494	0.389	2.32	0.426	3.89	4.26
D23[1]	0.69	6.24	0.464	0.370	2.31	0.446	3.62	4.46
D11[1]	0.83	9.00	0.463	0.369	2.25	0.308	4.05	3.08
D24[1]	0.70	6.07	0.442	0.356	2.04	0.438	3.20	4.38
D12[1]	0.83	8.85	0.457	0.365	2.03	0.310	3.38	3.10
D31[2]	1.00	12.0	0.431	0.348	1.72	0.216	4.19	2.16
D32[3]	0.99	9.41	0.355	0.298	1.37	0.226	3.40	2.26
D33[3]	1.07	7.83	0.261	0.229	1.24	0.200	3.05	2.00
D34[3]	1.09	6.04	0.198	0.179	1.13	0.196	2.89	1.96

Table 2
Runs, intermediate and shallow water depth $h = 25$cm ($h/D = 4.16$) (H131–H191) and $h = 15$cm ($h/D = 2.5$) (H262–H273). [1a] Violent breaking behind the cylinder; [1b]Violent breaking at the cylinder; [2]Weakly breaking; [3]Non-breaking.

run	T_{TT}[sec.]	$\eta_{0,m}$[cm]	$k\eta_{0,m}$	$Ru_m/\eta_{0,m}$	kD	$M_m/\rho g R^2\eta_{0,m}h$	kh
H131[1a]	0.92	9.90	0.543	2.24	0.328	3.76	1.37
H132[1b]	0.87	9.51	0.559	1.97	0.354	4.29	1.47
H121[2]	0.69	6.12	0.531	1.86	0.520	2.97	2.17
H141[2]	0.90	8.08	0.450	1.71	0.334	3.18	1.39
H151[3]	1.03	7.86	0.358	1.59	0.274	3.37	1.14
H111[2]	0.91	5.87	0.324	1.55	0.332	3.09	1.38
H161[3]	1.19	7.33	0.281	1.47	0.230	2.88	0.958
H171[3]	1.21	7.83	0.290	1.46	0.222	3.11	0.925
H191[3]	1.35	7.42	0.240	1.46	0.194	3.23	0.808
H181[3]	1.45	6.89	0.209	1.32	0.182	2.59	0.758
H262[3]	1.02	5.04	0.281	1.67	0.334	2.55	0.835
H263[2]	1.01	5.40	0.310	1.65	0.344	2.38	0.860
H273[2]	1.28	4.58	0.200	1.46	0.262	2.18	0.655
H283[2]	1.09	4.95	0.261	1.45	0.316	2.45	0.790
H282[3]	1.10	4.54	0.230	1.41	0.304	2.36	0.760
H272[3]	1.27	4.41	0.190	1.41	0.258	2.27	0.645

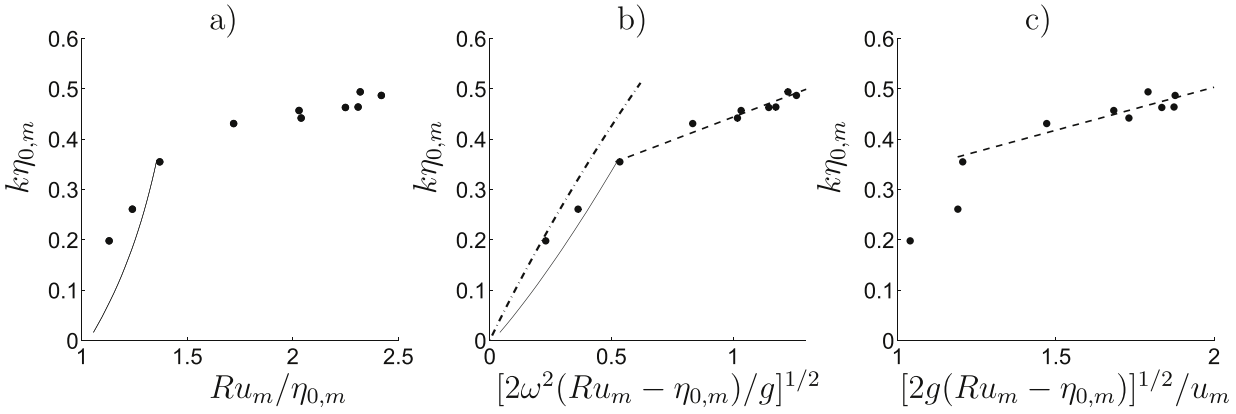

Fig. 3. a) Runup maximum $Ru_m/\eta_{0,m}$ at front face of the cylinder (at 0°), b) $[2\omega^2(Ru_m-\eta_{0,m})/g]^{1/2}$, c) $[2g(Ru_m-\eta_{0,m})]^{1/2}/u_m = M^{1/2}$vs. wave slope $k\eta_{0,m}$. Present measurements in focusing waves with $h/D = 10$(•). Second-order theory for periodic waves (WAMIT) with $h/D = \infty$ by Morris-Thomas and Thiagarajan (2004, Fig. 9c) (——). In plot b) u_m/c^{∞}_{ref} in Eq. (5) – · – . and $k\eta_m = 0.260 + 0.184\,[2\omega^2(Ru_m-\eta_{0,m})/g]^{1/2}$ (linear fit – – –). In plot c) $k\eta_m = 0.161 + 0.171\,[2g(Ru_m-\eta_{0,m})]^{1/2}/u_m$(linear fit – – –).

wave slope (of $k\eta_{0,m} = 0.355$). Beyond that, a different physics is taking place. This is not modelled by second-order theory. Rather, the behaviour and process are similar to, e.g., the orbital velocity in strongly nonlinear and breaking waves (Grue and Jensen, 2012, Fig. 9) and the strongly nonlinear Stokes drift (Lenain et al., 2019). In this range, the variable Z grows according to $k\eta_{0,m} = 0.260 + 0.184Z$ (linear fit). In Fig. 3b we have also plotted the horizontal speed below crest as obtained by (5). This is used to calculate the factor $M^{1/2}$ from the experiments obtaining $k\eta_{0,m} = 0.161 + 0.171M^{1/2}$ ($0.355 < k\eta_{0,m}$) (linear fit) with M up to 3.5 in the experiments in deep water ($h/D = 10$).

The second-order calculations by Morris-Thomas and Thiagarajan (2004) were supported by experiments where the latter were carried out at water depth to cylinder diameter ratio of $h/D = 5$, where the finite h also slightly modifies the wavenumber, and are discussed below.

3.2. Finite depth ($h/D \sim 2.5 - 5.36$)

Present experiments at intermediate and shallow depth were performed with $h/D = 4.16$ and 2.5. The nondimensional wavenumber is in the range $0.65 < kh < 2.17$. Values of kD are in the range 0.18–0.52 (Table 2).

Our experiments are compared to the large scale random wave experiments presented by method 3 in Garborg et al. (2019, table A11). We refer to their runup level B (see also section 2.1). They studied the runup in terms of the measured zero-down crossing period. The crest height was subsequently calculated by stream function theory for symmetrical waves. Their parameter range partially overlaps with the present experiments (Table 3). Another set of small scale measurements using wire gauges in regular waves by Morris-Thomas and Thiagarajan (2004, Fig. 9c) have parameters on the border of the present experiments, while a random wave event and periodic wave event in De Vos et al. (2007, Figs. 6 and 15) overlap present parameter range. Effects on wide cylinders computed by Buchmann et al. (2000, Fig. 9A) and Zhang and Teng (2017) are outside the range of present experiments.

Runup $Ru_m/\eta_{0,m}$ as function of $k\eta_{0,m}$ present and other experiments shows a great scatter (Fig. 4a). However, the function $Z =$

Table 3
Range of h/D, kh and kD of various experiments and calculations.

	h/D	kh	kD
Present	2.5 and 4.16	0.65–2.17	0.18–0.52
Garborg et al. test no. 1	5.36	2.6–3.1	0.49–0.58
Garborg et al. test no. 2	5.36	2.07	0.39
Garborg et al. test no. 3	3.57	1.55	0.43
Morris-Thomas and Thiagarajan, Fig. 9c	5	2.14	0.43
De Vos et al. Fig. 15	4.55	0.84	0.19
De Vos et al. Fig. 6	4.55	1.02	0.22
Buchmann et al., Fig. 9A	0.5	1	2
Zhang and Teng, Figs. 9 and 12	0.16–0.23	0.32–0.46	2

$[2\omega^2(Ru_m-\eta_{0,m})/g]^{1/2}$ is found to gather the data from the present experiments with $h/D=2.5$ and $h/D=4.16$ along one common line. This is given by $k\eta_{0,m}=0.0545+0.495Z$ (linear fit) and is shown by the dashed line in Fig. 4b. This behaviour is similar to the process at large wave slope, at great depth. Here, however, the threshold wave slope is small. Further, the growth rate at finite water depth is less strong compared to deep water. Note that $kh<2.17$ in present experiments. Runup of large scale test no. 3 of Garborg et al. has $h/D=3.57, kh=1.55$. Result for Z fits well with the present experiments. The same is true for their test no. 2 where $h/D=5.36, kh=2.07$. This is also true with the results by De Vos et al. where $h/D=4.55, kh\simeq 1$. Test no. 1 of Garborg et al. exhibits a systematic deviation in the sense that Z is much greater compared to present experiments, for same wave slope. Note that $kh\sim 2.6-3.1$ in Garborg et al.'s test no. 1 and is outside the range of present experiments. This implies wave conditions towards the deeper part of the intermediate depth range. That experiment illustrates a subtile part of the intermediate depth range where $kh\sim 3$, $\tanh(kh)\simeq 1$ and input waves are close to deep water waves, where, however, effects of a finite depth are present because $5<h/D<10$. Experiments (or computations) in this range may exhibit a linear relationship such as $k\eta_{0,m}=a+bZ$ where coefficients a,b are between those presented for $h/D\sim 2.5-5$ (Fig. 4b) and $h/D=10$ (Fig. 3b). Test no. 1 of Garborg et al. eventually suggests that the linear fit in Fig. 4b is valid with an upper bound of approximately $kh=2$.

The regular wave experiments of the runup obtained by wire gauges by Morris-Thomas and Thiagarajan (2004) had $h/D=5$ and $kh=2.14$ (and $kD=0.43$). Values of Z grow linearly with the wave slope at a somewhat stronger rate compared to present experiments. The runup on very wide cylinders in shallow water (Buchmann et al., Zhang and Teng) are larger compared the slender cylinders at intermediate depth. The corresponding Z-variable grows approximately linearly with the wave slope (Fig. 4b).

We have obtained the function $M^{1/2}$ for the present experiments ($1.6<M<2.3$). This shows a great scatter (Fig. 4c). The orbital velocity at crest (u_m) in (1) was obtained using Fenton's method for each single experiment.

Present results are useful for runup predictions by first obtaining from the input wave elevation the trough-to-trough period T_{TT} and wave crest maximum $\eta_{0,m}$ of the wave events. The wave slope estimate is determined by $k\eta_{0,m}$. Value of Z is obtained from $k\eta_{0,m}=a+bZ$ where coefficients a,b are obtained from the linear fits presented in the figures. Runup is eventually calculated by

$$Ru_m=\eta_{0,m}+\frac{1}{2}g(Z/\omega)^2,\quad \omega=2\pi/T_{TT}.$$

Predictions by the formula in the finite depth case, with $kh<2$, and $a=0.0545$ and $b=0.495$, compare to experiments with a relative accuracy of 10 percent or better (Fig. 5).

4. Runup velocity

The runup at positions 1–5 are obtained as function of time (Fig. 6). This is done by manual digitalization of the video recordings. A cubic polynomial least squares fit to the experimental recordings obtain the runup $Y_i(t)$ as a continuous and differentiable function. The runup velocity is obtained by taking the time derivative of $Y_i(t)$. The runup velocity is plotted against runup position where experiments at great depth are shown in Fig. 7 ($h/D=10$). The runup velocity is up to twice the wave propagation speed, in the strongest wave events. At a vertical level of 1.5 times the maximum crest height, the runup velocity greatly exceeds the wave propagation speed, still. Note that these great runup velocities occur in deep water conditions. The great runup velocities illustrate the physics of the strong runup process occurring at the large wave slopes (Fig. 3).

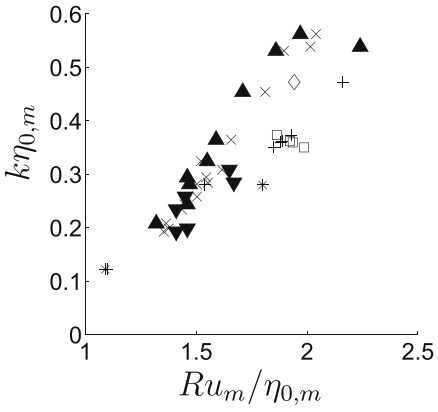

Fig. 5. Runup maximum $Ru_m/\eta_{0,m}$ at front face of the cylinder (at 0°). Present measurements (▲, ▼), formula × . Measurements by Garborg et al. (2019, Table A11), test no. 2 (□), test no. 3, (⋄), formula + . Measurements by De Vos et al. (∗), formula + .

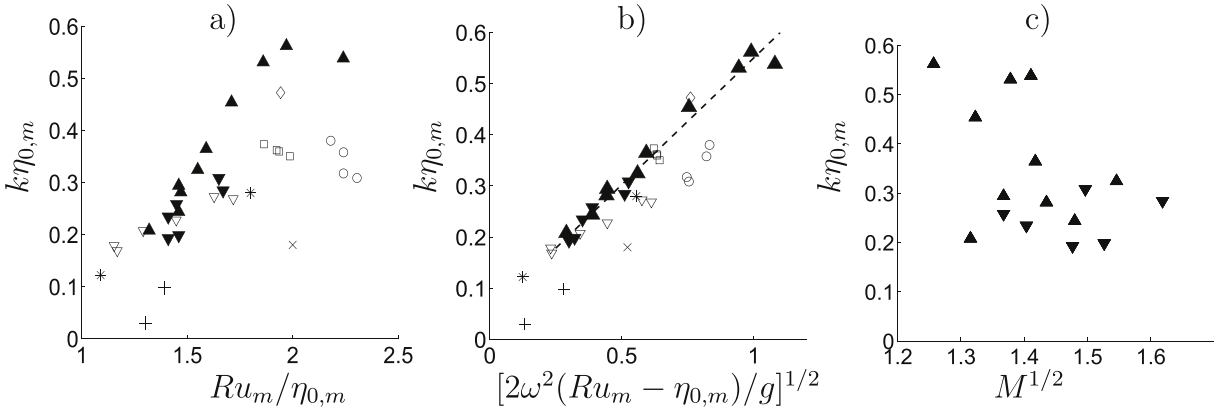

Fig. 4. a) Runup maximum $Ru_m/\eta_{0,m}$ at front face of the cylinder (at 0°), b) $[2\omega^2(Ru_m-\eta_{0,m})/g]^{1/2}$, c) $M^{1/2}$ vs. waveslope $k\eta_{0,m}$. Present small scale experiments with h/D = 4.16 (▲) and h/D = 2.5 (▼). Garborg et al. (2019, Table A11), test no. 1, $h/D=5.36$ (⋄), test no. 2, $h/D=5.36$ (□), test no. 3, $h/D=3.57$ (⋄). Experiments by De Vos et al. (2007, Figs. 6 and 15), $h/D=4.55$ (∗) and by Morris-Thomas and Thiagarajan (2004, Fig. 9c), $h/D=5$ (▽), Periodic 2nd order theory (Buchmann et al., 2000, Fig. 9(A)), $h/D=0.5$ (×), Cnoidal wave theory (Zhang and Teng, 2017), $h/D=1.2$ (+). Linear fit of present experiments, $k\eta_{0,m}=0.0545+0.495\,[2\omega^2(Ru_m-\eta_{0,m})/g]^{1/2}$ (− − −).

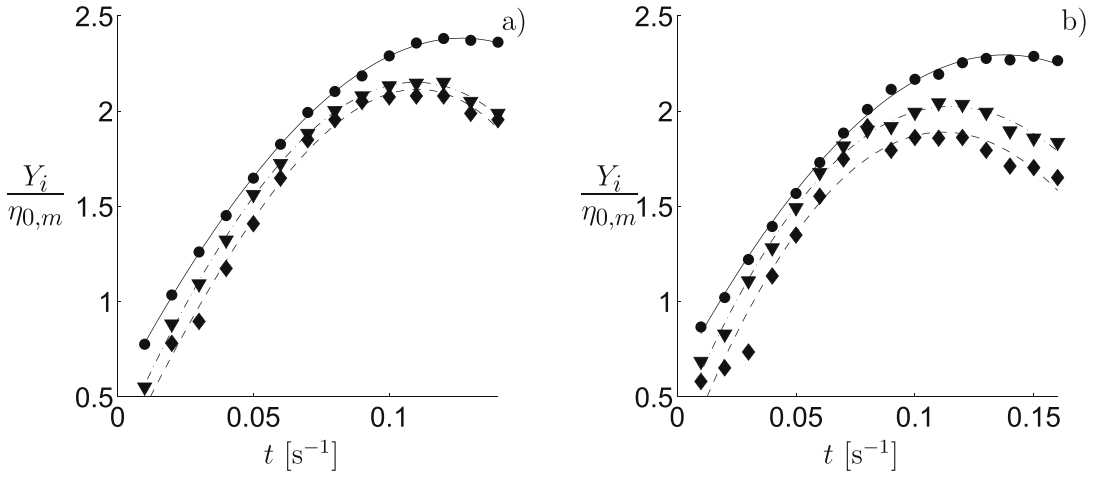

Fig. 6. Run-up $Y_i(t)$ vs. time. Measurement (black symbols) and cubic polynomial fit (lines). Pos. 1 at 0°(•, ——), Pos. 3 at 60° (▼, – · – ·), Pos. 5 at 90° (◆, – –). a) Run D21, b) D11.

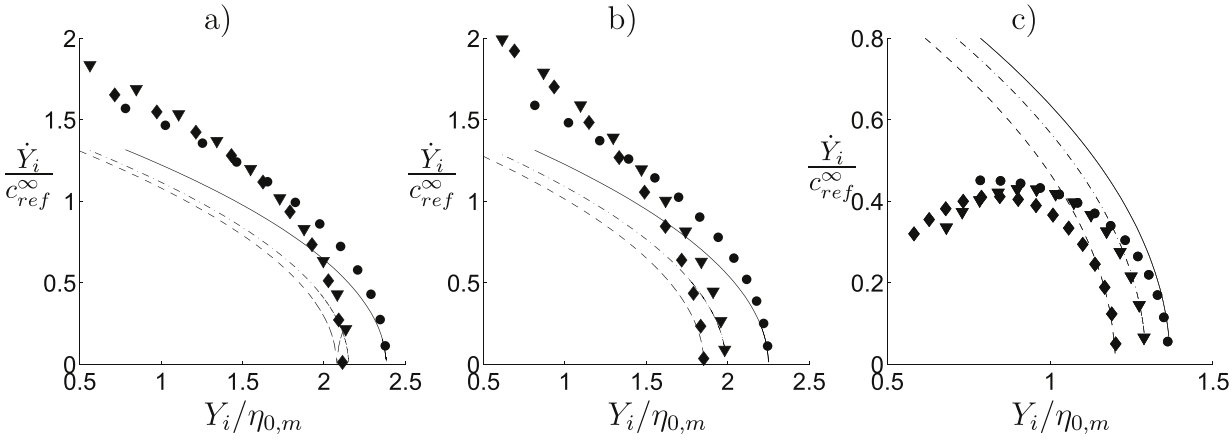

Fig. 7. Run-up velocity $\dot{Y}_i$vs. run-up position Y_i. Measured (black symbols), simplified model by $v_i(y) = \sqrt{2g(Y_{i,max} - y)}$ (lines). Pos. 1 at 0° (•, ——), Pos. 3 at 60° (▼, – · – ·), Pos. 5 at 90° (◆, – –). a) Run D21, b) D11, c) D32.

An estimate of the runup velocity may be obtained from a simplified energy like equation, see, e.g., Lykke Andersen et al. (2011),

$$(1/2)v_i(y)^2 = g\big(Y_{i,max} - y\big), \tag{7}$$

where y is the vertical coordinate of the runup. The approximation (7) fits well to the experimental velocities, close to runup maximum. The model (7) significantly underestimates the runup velocity when $\dot{Y}_i/c^{\infty}_{ref} > 0.5$, in the strong runs D21 and D11 at great water depth shown in Fig. 7a and b. Note that the input waves are very strong in the two cases, with $k\eta_{0,m} = 0.494$ and 0.463, respectively. In the weaker run D32, with $k\eta_{0,m} = 0.355$, the estimate (7) greatly overestimates the runup velocity when $\dot{Y}_i/c^{\infty}_{ref} \geq 0.3$ (Fig. 7c). Note that run D32 is at the border between the two different runup ranges illustrated in Fig. 3, where the physics of run D32 may be calculated by second-order diffraction method such as WAMIT.

At finite depth conditions ($h/D = 4.16, 2.5$), the runup velocity in five strong wave events are obtained in Fig. 8. The strongest run H131 is due to a nonbreaking wave at the cylinder position. The wave exhibits strong breaking right behind this position, however. This run has both the largest runup and largest runup velocity. The plot in Fig. 8a illustrates that the runup is somewhat larger at the weatherside (position 1 at 0°) compared to the other measurement positions, and that the runup velocity is the largest at the lateral position 5 at 90°. All among the remaining cases in Fig. 8 are driven by an input wave that, with the cylinder absent, breaks at the cylinder position.

Comparing the breaking wave runs H132 and H121, both of similar wave slope, the plot in Fig. 8d illustrates that the runup velocity is the greatest at position 5 at 90° in run H121 while Fig. 8b indicates a greatest runup velocity at positions 1 at 0° and 3 at 60° in run H132. The maximum runup velocity obviously depends on the position along the circumference, and on the local features of the breaking wave crest. The plots in Fig. 8 illustrate that the approximation (7) compares quite well to the runs at finite depth.

Consider the runup velocity evaluated at the level of the crest height ($y = \eta_{0,m}$). We plot this quantity versus the wave slope (Fig. 9). Results from the nine largest runs at great depth ($h/D = 10$) in Fig. 9a show a great scatter in $\dot{Y}_i/c^{\infty}_{ref}$ along the cylinder contour. However, the important point is the overall maximum runup velocity along the contour: $\max_i(\dot{Y}_i)/c^{\infty}_{ref}$. This shows a clear nonlinear growth with increasing wave slope, up to a maximum of 1.8 for $k\eta_{0,m} \simeq 0.464$. The runup velocity then decreases to $\max_i(\dot{Y}_i)/c^{\infty}_{ref} \simeq 1.5$ for the still steeper wave with $k\eta_{0,m} \simeq 0.494$. The approximation (7) overpredicts the runup velocity for the moderately steep waves and underpredicts for the steep waves ($h/D = 10$).

The runup velocity versus wave slope at finite depth ($h/D = 4.16$, 2.5) shows similar behaviour as at great depth. However, runup velocity

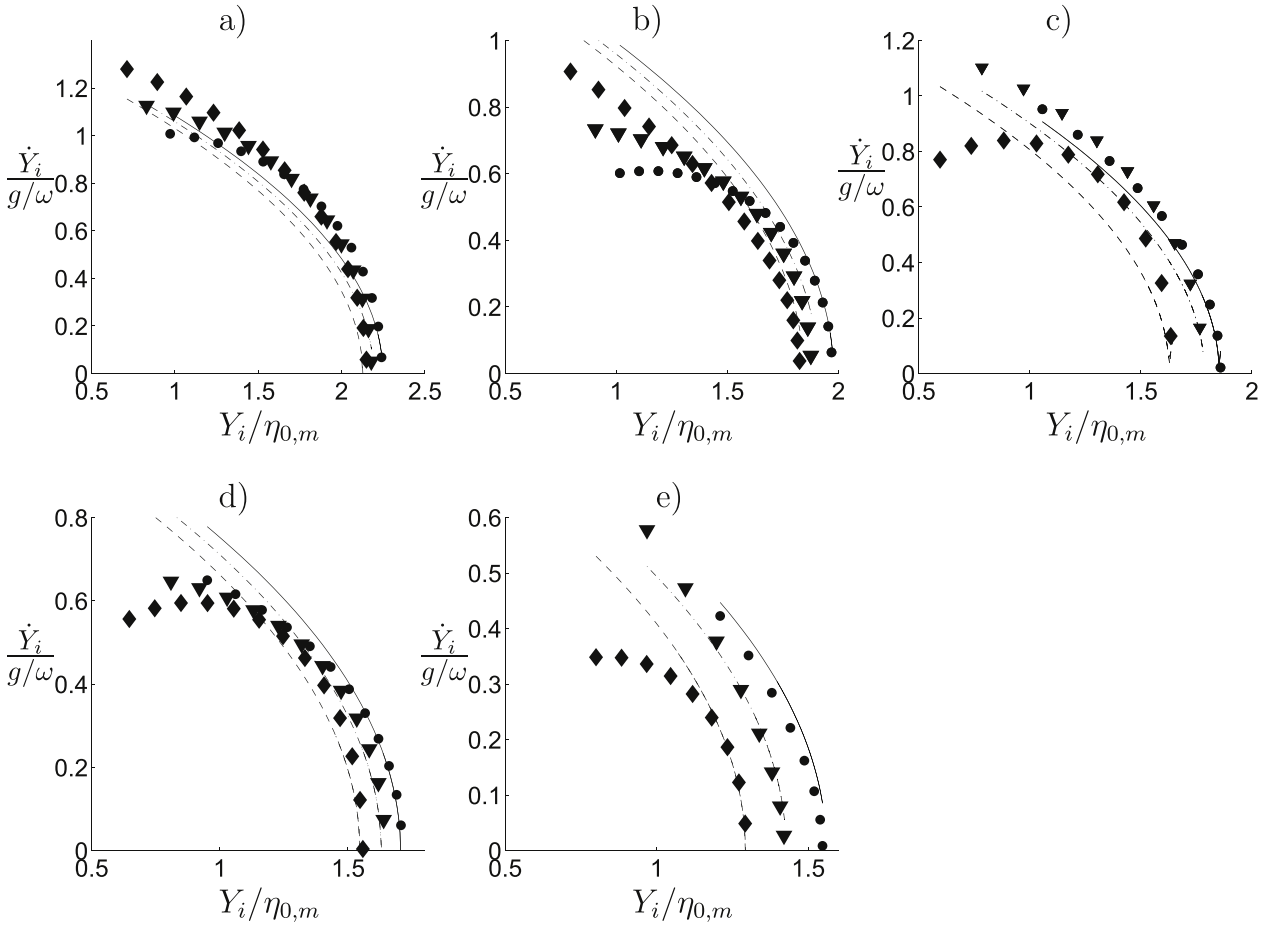

Fig. 8. Same as Fig. 7 but at finite depth. a) Run H131, b) H132, c) H121, d) H141, e) H111.

is less strong. The runup velocity grows to a nondimensional maximum of 1.2 for the wave in run H131 where the runup is also at maximum and where $k\eta_{0,m} = 0.543$. Note that the wave is nonbreaking in this event. The nondimensional runup velocity decays to a value slightly less than unity for the stronger run H132, where the wave is breaking, however, and $k\eta_{0,m} = 0.559$. Note that the breaking run H121 with $k\eta_{0,m} = 0.531$ exhibits a nondimensional runup velocity of 1.05 and is slightly greater than in the obviously stronger breaking run H132. The results illustrate that wave breaking reduces both runup height and runup velocity. At finite depth, the approximation (7) underpredicts the measurement by approximately 10 per cent in the strongest case.

5. Conclusion

By high speed camera technique we have filmed and quantified the runup on a slender cylindrical column exposed to long, steep waves, at finite water depth and in deep water. The ratio between the water depth and cylinder diameter was $h/D = 10$, 4.16 or 2.5. Large wave events were made using the focusing technique. In each event, the trough-to-trough period T_{TT} and crest elevation $\eta_{0,m}$ were obtained from the elevation time series at the position of the cylinder axis. The input waves were obtained in experimental runs with the cylinder absent. Frequency $\omega = 2\pi/T_{TT}$ and reference speed g/ω were defined for each event. Wavenumber was obtained from the dispersion relation.

Measurements of runup maximum are presented in terms of the variable $Z = [2\omega^2(Ru_m - \eta_{0,m})/g]^{1/2}$. This is investigated as function of the wave slope $k\eta_{0,m}$. Present results at finite water depth collapse along one common linear relationship:

$$k\eta_{0,m} = a + b\,Z, \quad k\eta_{0,m} < 0.56. \tag{8}$$

Coefficients $a = 0.0545$ and $b = 0.495$ were obtained by linear fit. This functional relationship is obtained for $h/D = 4.16$ and 2.5. Wavenumber times water depth is $kh < 2.17$, and $kD < 0.52$. Runup is eventually predicted from $\eta_{0,m}$, ω and Z by $Ru_m = \eta_{0,m} = \frac{1}{2}g(Z/\omega)^2$. Large scale experiments in random wave events with $h/D < 5.36$, $kh < 2.07$ and $kD < 0.4$, compare excellent to present results (Garborg et al., 2019, their tests no. 2 and 3). We refer to their runup level B (see section 2.1). The same is true for two random wave events with $h/D = 4.55$ and $kh \simeq 1$ (De Vos et al., 2007). Runup in regular waves was measured by wire-gauges by Morris-Thomas and Thiagarajan (2004). Parameters were $h/D = 5$, $kh = 2.14$, $kD = 0.43$, and cylinder draught to diameter ratio was 2.9 (the cylinder did not touch the bottom). The regular wave experiments partially overlap with present experiments. Values of Z obtained from the regular wave experiments somewhat exceed present experiments for $k\eta_{0,m} = 0.27$, however.

Random wave event in Garborg et al. (2019, their test no. 1) has parameters $h/D = 5.36$, $kh = 2.85 \pm 0.25$ and $kD = 0.53 \pm 0.04$. The wavelength is shorter than in the present experiments. This run by Garborg et al. suggests that present finite depth result with $k\eta_{0,m} = 0.0545 + 0.495\,Z$ is indeed valid up to a kh-value somewhere between 2 and 2.85. If the wavenumber kh is larger than this threshold, the growth of Z becomes stronger, and threshold wave slope becomes larger. Such a trend is confirmed by present experiments with $h/D = 10$ (and $2 < kh < 4.5$, $kD < 0.45$) where $k\eta_{0,m} = 0.260 + 0.184\,Z$ is valid for $0.355 < k\eta_{0,m}$. Further experiments with $5 < h/D < 10$ and $2.5 < kh < 4$ will help clarify the relationship between $k\eta_{0,m}$ and Z in the relatively shorter wave part of the intermediate depth range.

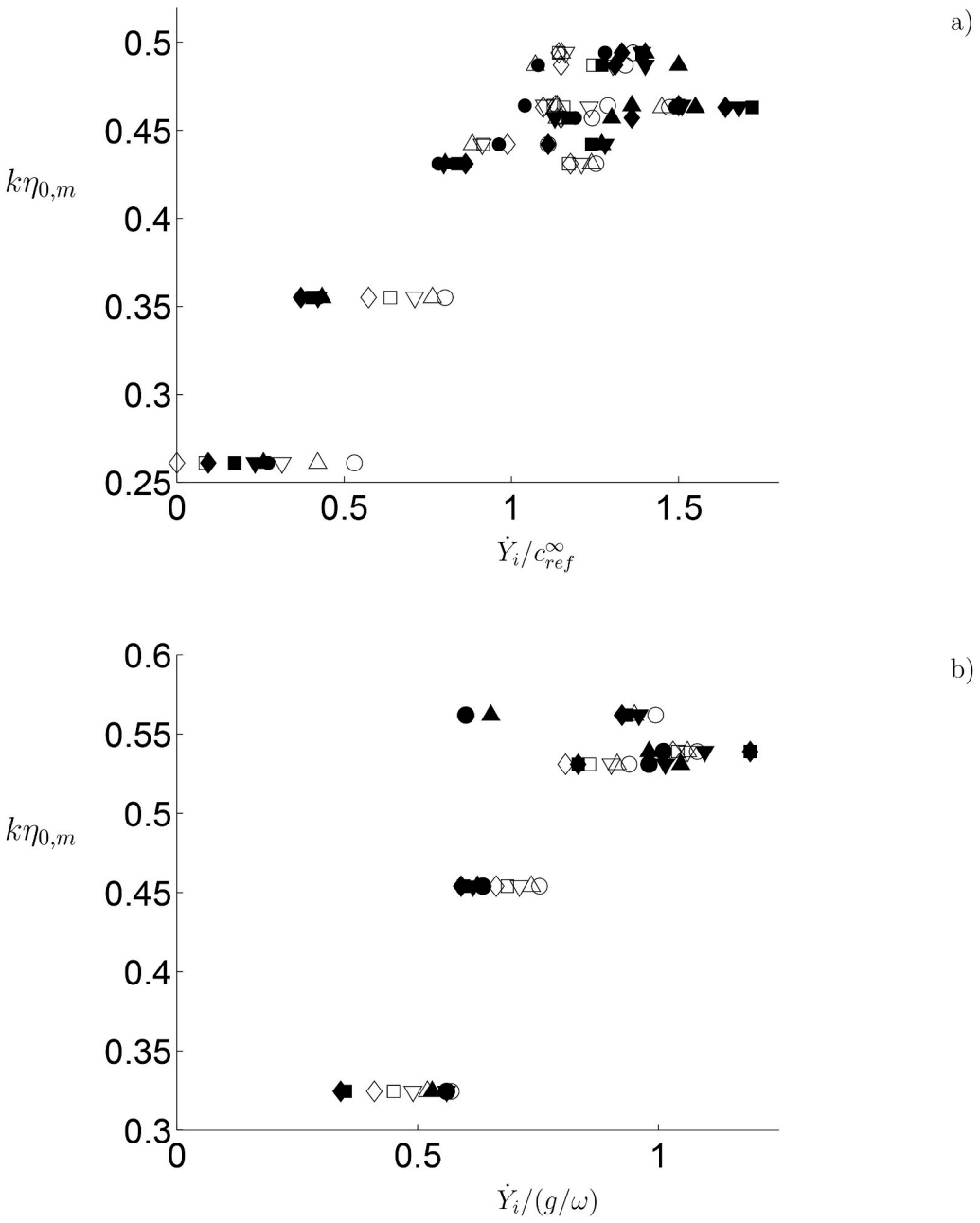

Fig. 9. Run-up velocity at $y = \eta_{0,m}$ vs. $k\eta_{0,m}$. a) great depth, b) finite depth. Measured: black symbols; formula (7) open symbols. Pos. 1 (0°) •◦; pos. 2 (41.4°) ▲△; pos. 3 (60°) ▼▽; pos. 4 (75.7°) ■□; pos. 5 (90°) ◆◇

Measured runup velocity shows a strongly nonlinear relationship with the wave slope. At the level of the crest height, the vertical runup velocity is up to 1.8 times the wave speed at maximum, at great water depth ($h/D = 10$), and up to 1.2 times the wave speed at finite depth ($h/D = 4.16, 2.5$). Strong, nonbreaking waves are found to give the largest runup and runup velocity and is documented by the experiments at finite depth. Estimate of the runup velocity by $v_i(y)^2 = 2g(Y_{i,max} - y)$, where i denotes the runup position along the cylinder circumference, is useful in the finite depth conditions. A deviation of up to 10 per cent from measured values is found. In the deep water cases ($h/D = 10$) this deviation is much greater, however.

Author statement

The experiments were performed by Bogdan Osyka, and presented in report form.

The text and reanalysis were prepared by John Grue.

The revision was prepared by John Grue with input of experimental details by Bogdan Osyka.

Declaration of competing interest

The authors declare that they have no known competing financial interests or personal relationships that could have appeared to influence the work reported in this paper.

Appendix A. Supplementary data

Supplementary data to this article can be found online at https://doi.org/10.1016/j.coastaleng.2020.103775.

References

Alberello, A., Chabchoub, A., Monty, J.P., Nelli, F., Lee, J.H., Elsnab, J., Toffoli, A., 2018. An experimental comparison of velocities underneath focussed breaking waves. Ocean Eng. 155, 201–210.

Baldock, T.E., Swan, C., Taylor, P.H., 1996. A laboratory study of nonlinear surface water waves. Philos. Trans. R. Soc. London, Ser. A 354, 649–676.

Bonakdar, L., Oumeraci, H., Etemad-Shahidi, A., 2016. Run-up on verical piles due to regular waves: small-scale model tests and prediction formulae. Coast. Eng. 118, 1–11.

Buchmann, B., Ferrant, P., Skourup, J., 2000. Run-up on a body in waves and current. Fully nonlinear and finite-order calculations. Appl. Ocean Res. 22, 349–360.

De Vos, L., Frigaard, P., De Rouck, J., 2007. Wave run-up on cylindrical and cone shaped foundations for offshore wind turbines. Coast. Eng. 54, 17–29.

Faltinsen, O.M., Landrini, M., Greco, M., 2004. Slamming in marine applications. J. Eng. Math. 48, 187–217.

Fenton, J.D., 1988. The numerical solution of steady water wave problems. Comput. Geosci. 13 (3), 357–368.

Garborg, K., Lykke Andersen, T., Skourup, J., Frigaard, P., 2019. A re-analysis of run-up levels for slender monopiles. Int. J. Ocean and Coastal Engng. Vol. 2 (1 and 2), 1950002.

Grue, J., Clamond, D., Huseby, M., Jensen, A., 2003. Kinematics of extreme waves in deep water. Appl. Ocean Res. 25, 355–366.

Grue, J., Jensen, A., 2012. Orbital velocity and breaking in steep random gravity waves. J. Geophys. Res. 117, C07013. https://doi.org/10.1029/2012JC008024.

Hallermeier, R.J., 1976. Nonlinear flow of wave crests past a thin pile. J. Waterways, Harbors and Coastal Engng. Division 102 (4), 365–377.

Kazeminezhad, M.H, Etemad-Shahidi, A, 2015. A new method for the prediction of wave sunup on vertical piles. Coastal Engineering 98, 55–64.

Lenain, L., Pizzo, N., Melville, W.K., 2019. Laboratory studies of Lagrangian transport by breaking surface waves. J. Fluid Mech. 876, R1. https://doi.org/10.1017/jfm.2019.244.

Lykke Andersen, T., Frigaard, P., Damsgaard, M.L., De Vos, L., 2011. Wave run-up on slender piles in design conditions - model tests and design rules for offshore wind. Coast. Eng. 58, 281–289.

Morris-Thomas, M.T., Thiagarajan, K.P., 2004. The run-up on a cylinder in progressive surface gravity waves: harmonic components. Appl. Ocean Res. 26, 98–113.

Myrhaug, D., Holmedal, L.E., 2010. Wave run-up on slender circular cylindrical foundations for offshore wind turbines in nonlinear random waves. Coast. Eng. 57, 567–574.

Newman, J.N., 1977. Marine Hydrodynamics. MIT press, 402 pp.

Ramirez, J.R., Frigaard, P., Lykke Andersen, T., De Vos, L., 2013. Large scale model test investigation on wave run-up in irregular waves at slender piles. Coast. Eng. 72, 69–79.

Stansberg, C.T., Gudmestad, O.T., Haver, S.K., 2006. Kinematics under extreme waves. J. Offshore Mech. Arctic Eng. 130 (2), 021010.

Stansberg, C T, Baarholm, R, Kristiansen, T, Hansen, W W M, Rortveit, G, 2005. Extreme wave amplification and impact loads on offshore structures. Offshore Technology Conference. Houston, TX, USA, 2-5 May 2005, OTC 17487.

Zhang, J., Teng, B., 2017. Numerical study on cnoidal wave run-up around a vertical circular cylinder. Appl. Ocean Res. 63, 276–287. https://doi.org/10.1016/j.apor.2017.01.006.